Nanoscale

Dynamic Article Links

Cite this: *Nanoscale*, 2012, **4**, 4190

www.rsc.org/nanoscale

PAPER

Theoretical analysis of the optical excitation spectra of silver and gold nanowires†

Emilie B. Guidez and Christine M. Aikens*

Received 1st February 2012, Accepted 18th March 2012
DOI: 10.1039/c2nr30253e

The excitation spectra of linear atomic chains of silver and gold with various sizes have been calculated using time-dependent density functional theory. Silver chains show longitudinal and transverse peaks as well as a low-intensity d-band. The longitudinal peak, corresponding to the HOMO–LUMO transition (along the main axis of the chain), shifts linearly to the red as the length of the system increases, consistent with the particle-in-a-box model. The transverse peak remains at approximately constant energy for all systems studied and corresponds to $\sum_m \rightarrow \Pi_m$ transitions in the *xy* plane perpendicular to the chain. As the chain grows, transitions arising from d orbitals contribute to the transverse peak, which affects its oscillator strength. Contrary to silver, gold chains display a strong d-band that converges to a distinct pattern at a chain length of about twelve atoms. The transitions involved in the d-band originate from localized d-orbitals with a d_{z^2} character since they have the right symmetry to give transitions into the LUMO, LUMO + 1, …, which have $\sum$ symmetry. Transitions arising from these localized d-orbitals also affect the position of the longitudinal peak and generate a wide transverse band. Although the majority of the transitions involved in the transverse band have a $d\sum \rightarrow \Pi$ or $d\Pi \rightarrow \sum$ character, they are hidden by much stronger excitations of $d\Pi \rightarrow \Pi$ character in gold nanowires.

Introduction

Noble metal nanoparticles (*e.g.* Ag, Au) have been recently studied for applications in sensing,[1,2] catalysis[3] as well as the environmental[4] and biomedical fields.[5–8] One of the attractive properties of 10–100 nm noble metal nanoparticles is that they show a strong absorption peak in the visible-IR region that can be tuned by varying their size,[9] shape,[10,11] or chemical environment.[12] This is due to the concerted excitation of the conduction electrons in the presence of an electric field, or surface plasmon resonance (SPR).[13–17] As the nanoparticle size decreases (down to hundreds of atoms), molecular properties arise and the absorption spectrum becomes more complex. Quantum-mechanical calculations have been used to model the optical properties of noble metal clusters. In particular, time-dependent density functional theory (TDDFT) has been shown to provide insights regarding the origin of the discrete absorption spectra of noble metal clusters.[18–22] Molecular excitations obtained with TDDFT for small clusters show intense peaks analogous to the plasmon excitations of larger nanoparticles and correspond well with peaks described in the Mie theory framework or with other classical electrodynamics methods.[21,23] For example, tetrahedral Ag_{20} exhibits an intense peak that arises from a collective sp → sp intraband transition.[21]

Significant progress has been achieved in synthesizing gold and silver nanoparticles with a wide variety of shapes including spherical,[24] cylindrical,[25] decahedral,[26] icosahedral,[27] and triangular.[28] Cylindrical nanoparticles (nanorods and nanowires) are of particular interest since their optical properties are very sensitive to their aspect ratio.[15,29,30] Studies of linear atomic chains of alkaline metals (Na, K) and noble metals (Ag, Au) showed two main plasmon resonances: a longitudinal mode along the main axis of the chain and two transverse modes perpendicular to that axis.[31,32] The energy and intensity of the longitudinal mode can be tuned by changing the length of the chain. The two transverse modes correspond to plasmon resonances at the end-atoms and inner atoms of the chain respectively. Therefore, the behavior of the electrons on the more exposed end-atoms is very distinct from the central atoms. The transverse plasmon resonance of gold nanowires was previously shown to strongly enhance two-photon absorption.[33] Both alkaline metals and noble metals have a single electron in their valence shell. However, d electrons affect the plasmon resonance of the noble metal clusters, especially for gold due to relativistic effects.[22,34,35]

The aim of this work is to compare the absorption spectra of gold and silver nanowires (NWs), here defined as a linear chain of atoms, using time-dependent density functional theory and show how they are affected by the length of the nanowires. Orbitals

Department of Chemistry, Kansas State University, 213 CBC Building, Manhattan, KS 66506, USA. E-mail: cmaikens@ksu.edu

† Electronic supplementary information (ESI) available. See DOI: 10.1039/c2nr30253e

involved in the main longitudinal and transverse excitations are discussed in detail for both silver and gold nanowires.

Computational details

All calculations in this work are performed with the Amsterdam Density Functional (ADF) package.[36] All the geometry optimizations are run using the generalized gradient approximation (GGA) Becke–Perdew (BP86) exchange-correlation functional[37,38] and an all-electron double-zeta (DZ) basis set. Scalar relativistic effects are included with the zeroth-order regular approximation (ZORA).[39,40] In order to have closed-shell species, positively and negatively charged species are considered for nanowires with an odd number of atoms. Excitation spectra are calculated using time-dependent density functional theory (TDDFT) with the statistical average of orbital potentials (SAOP)[41] and LB94[42] model potentials. An all-electron double-zeta basis set is used for the SAOP calculations. With the LB94 potential, a frozen core is considered and the basis set used is DZ.4p for silver and DZ.4f for gold (henceforth abbreviated as DZ for both atoms). The absorption spectra are convoluted with a Gaussian with a full width at half maximum of 0.2 eV. Orbitals are represented with a contour value of 0.02.

Results and discussion

Silver nanowires

The excitation spectra of silver nanowires are analyzed in this section. The spectra of the neutral silver nanowires are analyzed first at the SAOP/DZ and LB94/DZ levels of theory, followed by a comparison with the positively and negatively charged nanowires.

(1) Neutral nanowires. The absorption spectra of silver nanowires Ag_n ($n = 2, 4, 8, 10, \ldots, 20$, and 40) show three distinct features: a sharp low-energy longitudinal peak, a low-intensity d-band and a transverse peak at about 6.3 eV (197 nm). The excitation spectrum of Ag_{20} is presented in Fig. 1A. The rest of the spectra are shown in the ESI†. The longitudinal peak corresponds to the HOMO → LUMO transition ($\Sigma \rightarrow \Sigma$). At the SAOP/DZ level of theory, this peak red shifts linearly from about 358 nm (3.46 eV) to 1562 nm (0.79 eV) as the length of the wire chain increases, as shown in Fig. 2A. The linear shift of the longitudinal peak is in accordance with the particle-in-a-cylinder model, as previously discussed by Johnson and Aikens.[43] A similar linear relationship is observed at the LB94/DZ level of theory but with a slightly smaller magnitude (Fig. 2A). It should also be noted that the transition energies tend to occur at higher wavelength with the exchange-correlation model LB94 than with SAOP as previously observed elsewhere.[21,43] An analogous red-shift of the longitudinal absorption peak with increasing aspect ratio is observed for noble metal nanowires synthesized experimentally.[44,45] As the aspect ratio increases, the energy of this peak tends to zero and its wavelength increases. Nanowires with very high aspect ratios can be transparent in the visible and near-IR regions.[45] In the linear atomic chains, the HOMO–LUMO gap will eventually approach zero which means that the system will become metallic as in the bulk material.

The HOMO and LUMO orbitals both have a strong delocalized s character as shown for Ag_6 in Fig. 3. These delocalized orbitals originate from the linear combination of the single 5s electron of the silver atoms. Since the 5s orbital of silver lies much higher in energy than the 4d orbitals, the HOMO–LUMO transitions are well defined and separated from the rest of spectrum (about 1.1 eV gap for Ag_{20}). We also note that the HOMO–LUMO transition starts splitting at a chain length of six atoms due to some contribution of the HOMO − 2 → LUMO transition, which is close in energy. As the nanowires grow longer, the splitting between the two peaks becomes smaller. The intensity of the longitudinal peak varies linearly with the length of the wire (and thus the number of electrons), as shown in Fig. 4. The peak intensities tend to be somewhat higher at the LB94/DZ level of theory but follow the same trend.

In the nanowire case, the longitudinal peak corresponds to a single HOMO–LUMO excitation. On the other hand, the longitudinal peak of silver nanorods with a larger diameter arise from several transitions involving delocalized orbitals.[43] For example for pentagonal Ag_{25}^{1+}, the strong longitudinal peak appears at 3.40 eV and corresponds to a linear combination of three "single-particle transitions" (a term referring to an electronic transition between an occupied and an unoccupied orbital) of $\Pi \rightarrow \Pi$ (HOMO − 1 → LUMO + 4) and $\Sigma \rightarrow \Sigma$ (HOMO − 2 → LUMO and HOMO − 2 → LUMO + 2) character.[43] The HOMO–LUMO transition is not allowed by symmetry.[43] The mixed transition at 3.40 eV arises when the *z*-components of the transition dipole moment combine in-phase; two weak peaks at 1.85 eV and 2.07 eV also arise from a linear combination of the same three single-particle transitions but have low oscillator strength and are not observable in the excitation spectrum because of a destructive interference of the transition dipole

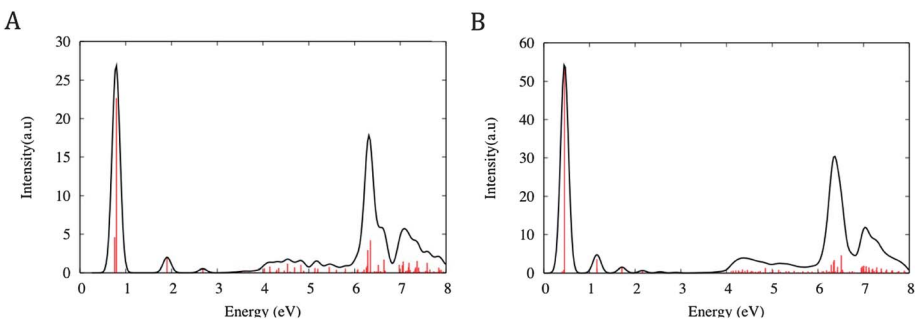

Fig. 1 Excitation spectra of (A) Ag_{20} nanowire and (B) Ag_{40} nanowire at the SAOP/DZ level of theory.

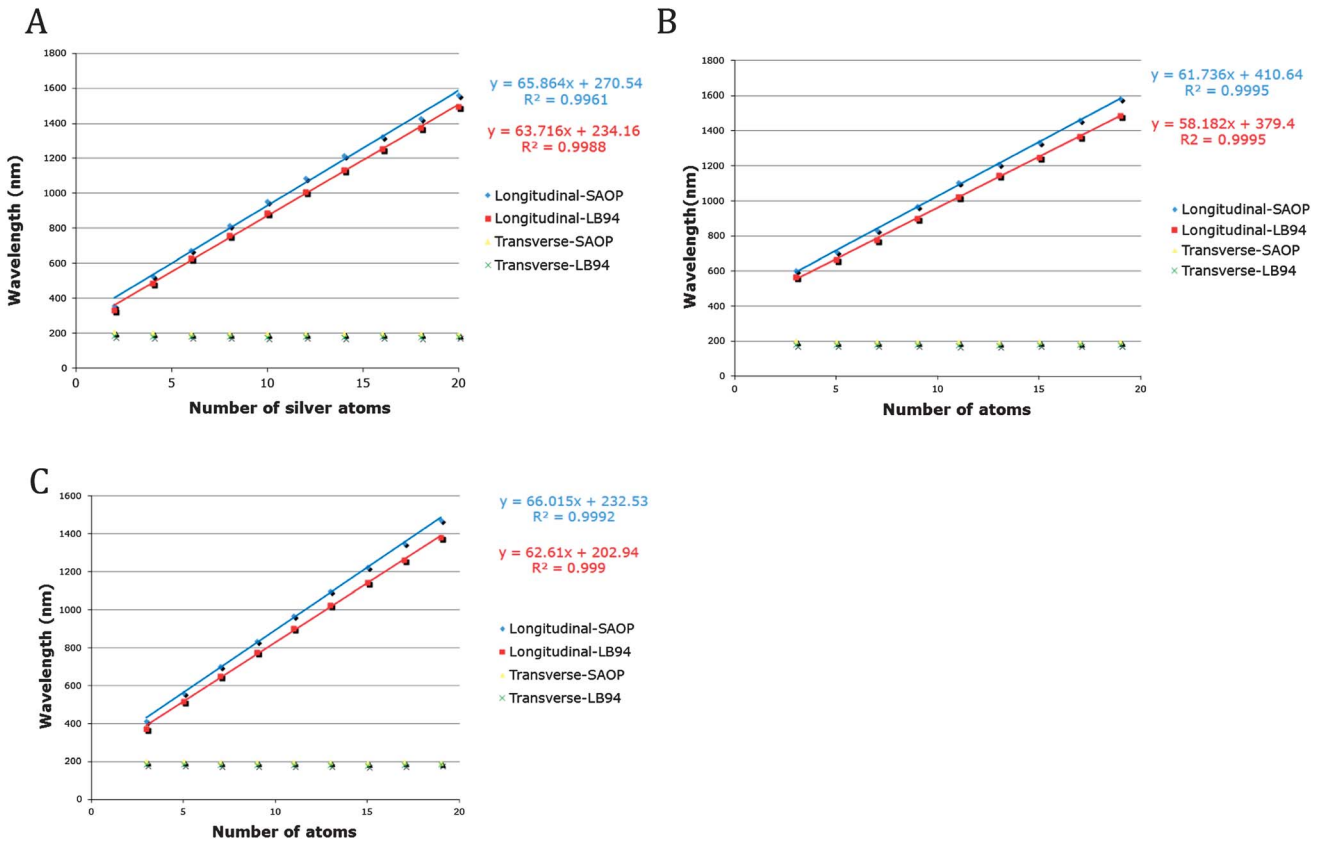

Fig. 2 Longitudinal and transverse peak wavelengths (nm) for (A) neutral (B) positively charged and (C) negatively charged silver nanowires.

moments.[43] The coupling between those transitions and the mechanism by which they form a single peak is yet to be understood, but appears to be the key factor in connecting the excitations of smaller clusters with the plasmon resonance of larger nanoparticles. The longitudinal peak for the nanowires examined in this work corresponds mainly to a single excitation, leading to a very sharp single peak. The peak assigned as plasmon for larger systems involves more transitions leading to broadening of the peak, especially for systems with partially filled shells.[21,43] Thus, it appears that a plasmon may be understood as a combination of single-particle transitions that constructively interact; in addition, multiple peaks in the same energy region can contribute. It is also important to note that we can expect the electron density of these nanorods in the excited state to be delocalized on the surface similar to the surface plasmon resonance, as explained by Harb *et al.* for spherical silver clusters.[23]

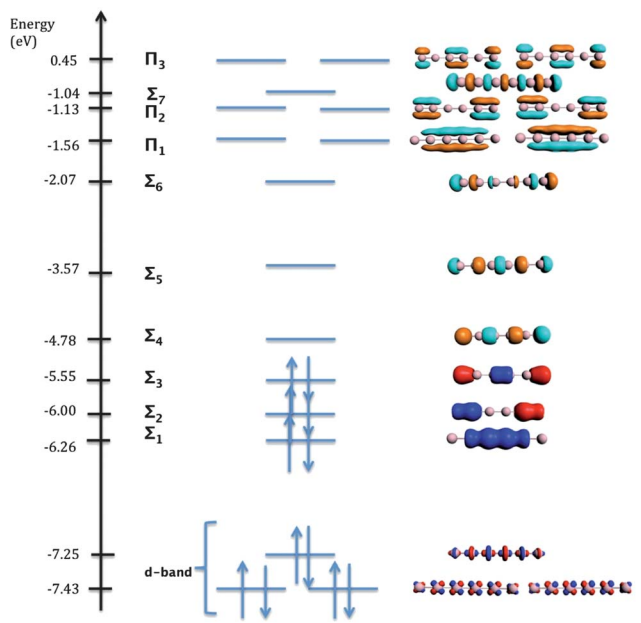

Fig. 3 Kohn–Sham orbital energy diagram of Ag_6 at BP86/DZ level of theory.

The next transition observed for the small nanowires Ag_n ($4 \leq n \leq 8$) corresponds to a transition out of the d-band. The energy between the start of the d-band and the HOMO–LUMO peak varies between 1.56 eV (Ag_4) and 1.73 eV (Ag_8). For the larger nanowires Ag_n ($10 \leq n \leq 20$), a second longitudinal peak appears below the d-band transitions. Its energy lies between 1.1 eV (Ag_{20}) and 1.6 eV (Ag_{10}) higher than the HOMO–LUMO peak. As the nanowires grow longer, energy gaps become smaller due to the increased number of interactions between the orbitals. Therefore, additional peaks appear and a greater number of d-band transitions are revealed. However, the intensities and energies of the d-band transitions remain constant, contrary to the main longitudinal peak. The d-orbitals are localized as shown in Fig. 3. As a result, the energies and intensities of the transitions originating from these orbitals are not greatly affected by the size of the nanowires. The d-band also appears smaller as the nanowires grow longer since the intensity of the main longitudinal

peak increases uniformly with the chain length. For very long nanowires, the d-band practically disappears as observed in the Ag_{40} case (Fig. 1B) in which only the longitudinal and transverse peaks can be seen. This is in accordance with what is observed experimentally for silver nanorods with diameters in the several-tens of nanometers range.[46]

The transverse peak corresponds to transitions in the *xy* plane ($\sum_m \rightarrow \Pi_m$, where *m* is the principal quantum number). Since the diameter of the nanowires does not change, the energy of this peak remains relatively constant, only varying between 6.1 eV (204 nm) and 6.4 eV (195 nm) at the SAOP/DZ level of theory, as shown in Fig. 2A. As discussed previously, transitions are shifted to smaller wavelengths with LB94/DZ and the energy of the transverse peak varies between 6.6 eV (186 nm) and 6.9 eV (178 nm). Table 1 shows the transitions involved in the main transverse peak at the SAOP/DZ level of theory. For Ag_n, the number of $\sum_m \rightarrow \Pi_m$ transitions is $n/2$. Therefore, the longer the nanowires are, the higher the number of transitions that can contribute to the transverse peak. For instance, the transverse peak of the nanowire Ag_8 has contributions from $\sum_1 \rightarrow \Pi_1$, $\sum_2 \rightarrow \Pi_2$, $\sum_3 \rightarrow \Pi_3$ and $\sum_4 \rightarrow \Pi_4$. The oscillator strength for each transition adds constructively. For $n \geq 10$, the trend continues but only the first few transitions are shown in the table. Additionally, we can see that the transverse peak has a large intensity (at least three times as large as the d-band). Although the intensity of the peak generally increases with length, it shows some oscillations as shown in Fig. 4B. It should be noted that this oscillatory behavior is a little different at the LB94/DZ level of theory (Fig. 4D). These oscillations can be explained by some contributions of the d-band to the peak. In fact, starting at a length of six atoms, d-transitions start to mix with the $\sum_m \rightarrow \Pi_m$ transverse transitions as shown in Table 1. Although the main contribution to the dipole moment originates from $\sum_m \rightarrow \Pi_m$ transitions, the weights of the d-transitions that participate are large enough that the contribution to the peak intensity is non-negligible. However, in general the d-band contribution to the dipole moment is rather small.

(2) Positively and negatively charged nanowires. The absorption spectra of the positively charged silver nanowires Ag_n^+ ($n = 3, 5, 7, 9, \ldots, 19$) and their negatively charged counterparts Ag_n^- ($n = 3, 5, 7, 9, \ldots, 19$) share many similar features with the spectra of the neutral nanowires: they also have a longitudinal peak corresponding to the HOMO–LUMO transition, a low-intensity d-band, and a transverse peak that corresponds to one or more $\sum_m \rightarrow \Pi_m$ transitions. We note that the HOMO–LUMO gap of the positively charged nanowires decreases much slower than the HOMO–LUMO gaps obtained for the neutral and negatively charged species. In fact, the slope of the absorption wavelength of the longitudinal peak is

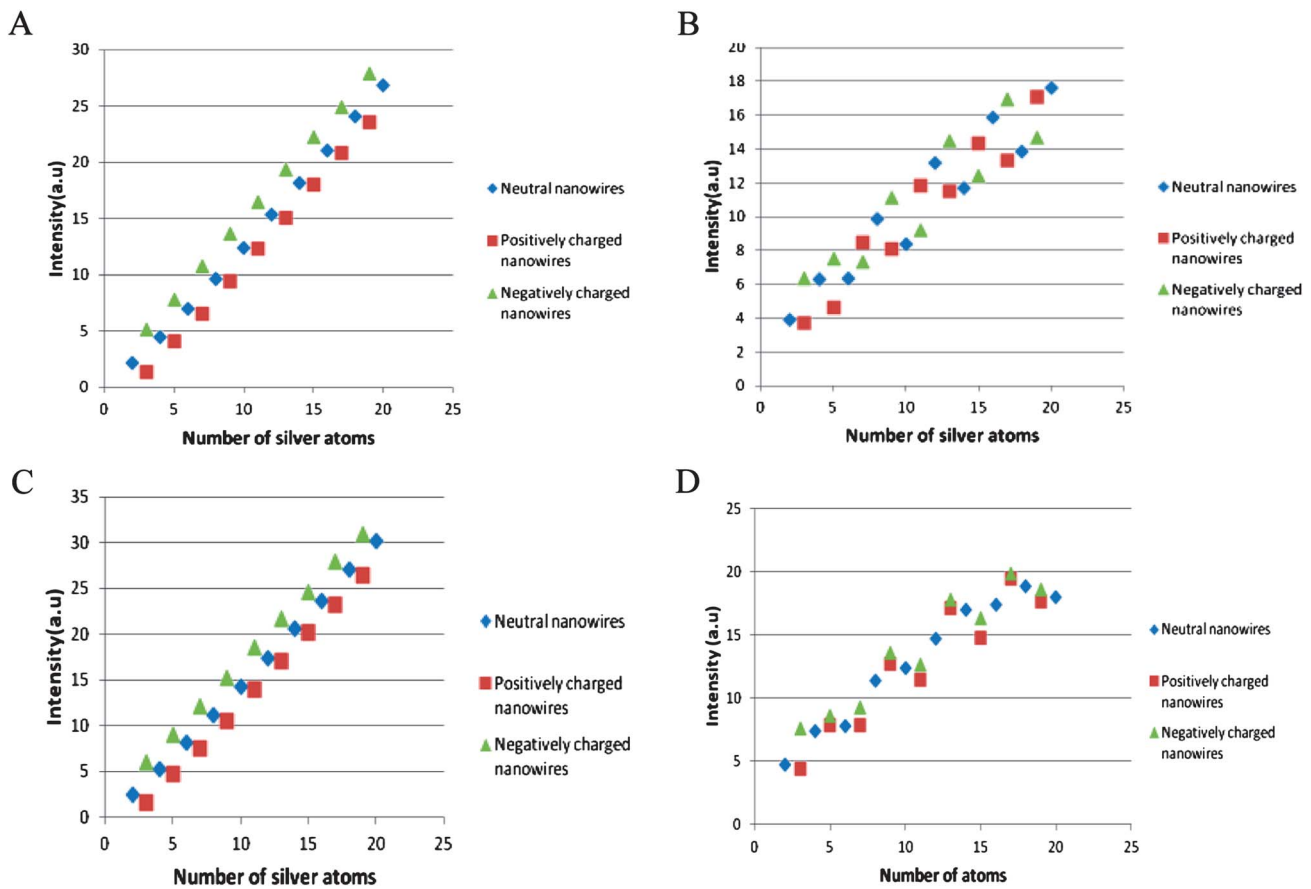

Fig. 4 Oscillator strength of (A) the longitudinal peak of silver nanowires with SAOP/DZ; (B) the transverse peak of silver nanowires with SAOP/DZ; (C) the longitudinal peak of silver nanowires with LB94/DZ; and (D) the transverse peak of silver nanowires with LB94/DZ. The maximum intensity of the Gaussian convolution was considered.

Table 1 Transitions contributing to the high-intensity transverse peak in silver nanowires at the SAOP/DZ level of theory

Ag_n	Energy (eV)	Transitions	Type of transition	Weight	Contribution to dipole moment
2	6.06	$10\sigma^+_g(\text{HOMO}) \rightarrow 6\pi_u$	$\sum_1 \rightarrow \Pi_1$	0.9269	2.2276
4	6.17	$19\sigma^+_u(\text{HOMO}) \rightarrow 11\pi_g$	$\sum_2 \rightarrow \Pi_2$	0.4742	−1.5740
		$19\sigma^+_g(\text{HOMO}-1) \rightarrow 11\pi_u$	$\sum_1 \rightarrow \Pi_1$	0.3838	−1.4066
6	6.20	$13\pi_u \rightarrow 30\sigma^+_g$	d-Band	0.4017	−0.1888
		$29\sigma^+_g(\text{HOMO}) \rightarrow 17\pi_u$	$\sum_3 \rightarrow \Pi_3$	0.1873	0.9849
		$28\sigma^+_u(\text{HOMO}-1) \rightarrow 16\pi_g$	$\sum_2 \rightarrow \Pi_2$	0.1340	0.8309
		$28\sigma^+_g(\text{HOMO}-2) \rightarrow 16\pi_u$	$\sum_1 \rightarrow \Pi_1$	0.1071	0.7391
8	6.29	$37\sigma^+_u(\text{HOMO}-2) \rightarrow 22\pi_g$	$\sum_2 \rightarrow \Pi_4$	0.2632	0.1029
		$38\sigma^+_u(\text{HOMO}) \rightarrow 22\pi_g$	$\sum_4 \rightarrow \Pi_4$	0.1583	0.8980
		$37\sigma^+_g(\text{HOMO}-3) \rightarrow 21\pi_u$	$\sum_1 \rightarrow \Pi_1$	0.1036	0.7217
		$37\sigma^+_u(\text{HOMO}-2) \rightarrow 21\pi_g$	$\sum_2 \rightarrow \Pi_2$	0.0971	0.7008
		$38\sigma^+_g(\text{HOMO}-1) \rightarrow 22\pi_u$	$\sum_3 \rightarrow \Pi_3$	0.0909	0.6796
10	6.25	$21\pi_g \rightarrow 49\sigma^+_u$	d-Band	0.4215	−0.2309
		$22\pi_g \rightarrow 49\sigma^+_u$	d-Band	0.1269	0.1588
		$48\sigma^+_g(\text{HOMO}) \rightarrow 28\pi_u$	$\sum_5 \rightarrow \Pi_5$	0.1106	0.7517
		$47\sigma^+_u(\text{HOMO}-1) \rightarrow 27\pi_g$	$\sum_4 \rightarrow \Pi_4$	0.0938	0.6919
12	6.26	$27\pi_g \rightarrow 59\sigma^+_u$	d-Band	0.3018	0.0745
		$57\sigma^+_g(\text{HOMO}-1) \rightarrow 34\pi_u$	$\sum_5 \rightarrow \Pi_7$	0.1418	0.1009
		$57\sigma^+_u(\text{HOMO}) \rightarrow 33\pi_g$	$\sum_6 \rightarrow \Pi_6$	0.1061	−0.7348
		$57\sigma^+_g(\text{HOMO}-1) \rightarrow 33\pi_u$	$\sum_5 \rightarrow \Pi_5$	0.0806	−0.6399
14	6.27	$30\pi_u \rightarrow 69\sigma^+_g$	d-Band	0.4543	0.2564
		$67\sigma^+_g(\text{HOMO}) \rightarrow 39\pi_u$	$\sum_7 \rightarrow \Pi_7$	0.0401	−0.4511
		$31\pi_u \rightarrow 69\sigma^+_g$	d-Band	0.0896	−0.1321
		$66\sigma^+_u(\text{HOMO}-1) \rightarrow 38\pi_g$	$\sum_6 \rightarrow \Pi_6$	0.0346	−0.4185
16	6.28	$36\pi_u \rightarrow 79\sigma^+_g$	d-Band	0.3422	−0.0875
		$76\sigma^+_u(\text{HOMO}) \rightarrow 45\pi_g$	$\sum_8 \rightarrow \Pi_{10}$	0.1085	−0.0582
		$76\sigma^+_u(\text{HOMO}) \rightarrow 44\pi_g$	$\sum_8 \rightarrow \Pi_8$	0.0720	0.6037
		$76\sigma^+_g(\text{HOMO}-1) \rightarrow 44\pi_u$	$\sum_7 \rightarrow \Pi_7$	0.0599	0.5499
18	6.28	$38\pi_g \rightarrow 88\sigma^+_u$	d-Band	0.4372	−0.2608
		$39\pi_g \rightarrow 88\sigma^+_u$	d-Band	0.1469	0.1669
		$86\sigma^+_g(\text{HOMO}) \rightarrow 50\pi_u$	$\sum_9 \rightarrow \Pi_9$	0.0519	0.5125
		$85\sigma^+_u(\text{HOMO}-1) \rightarrow 49\pi_g$	$\sum_8 \rightarrow \Pi_8$	0.0457	0.4804
20	6.34	$44\pi_g \rightarrow 98\sigma^+_u$	d-Band	0.4078	−0.0984
		$49\pi_g \rightarrow 99\sigma^+_u$	d-Band	0.0564	−0.0071
		$43\pi_g \rightarrow 98\sigma^+_u$	d-Band	0.0553	0.1042
		$91\sigma^+_g \rightarrow 55\pi_u$	d-Band	0.0490	0.0028
		$95\sigma^+_u(\text{HOMO}) \rightarrow 55\pi_g$	$\sum_{10} \rightarrow \Pi_{10}$	0.0376	−0.4333
		$95\sigma^+_g(\text{HOMO}-1) \rightarrow 55\pi_u$	$\sum_9 \rightarrow \Pi_9$	0.0356	−0.4215

distinctively smaller for positively charged nanowires, as shown in Fig. 2. Fig. 4A and C show that the more negatively charged the nanowires is, the larger the intensity of the longitudinal peak. This may be explained by the larger electron density for the negative species.

On the other hand, the energy of the transverse peak is not very affected by the charge of the nanowires. The intensity of the transverse peak shows similar oscillations for the positively charged and negatively charged species as those encountered for the neutral species (Fig. 4B and D). The energy and intensity of the d-based transitions are also not affected by the charge of the nanowires, which can be explained by the fact that the d orbitals are localized.

Gold nanowires

In this section, the absorption spectra of gold nanowires are analyzed and compared with their silver analogs. The absorption

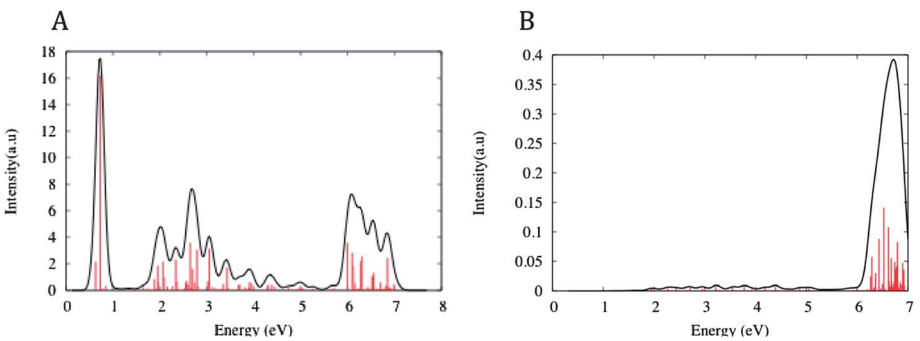

Fig. 5 (A) SAOP/DZ excitation spectrum of Au_{20} nanowire. (B) Subset of SAOP/DZ transverse excitation modes for Au_{20} nanowire.

spectra of gold nanowires also exhibit longitudinal and transverse peaks as well as transitions arising from the d-band, as shown with Au_{20} in Fig. 5A. The spectra of the neutral species are first discussed with an additional focus on the d-band, followed by a brief comparison with the positively charged and negatively charged species.

(1) Neutral gold nanowires. Contrary to the silver case, transitions originating from the d-band are important for the gold nanowires since they highly affect the longitudinal and transverse peak energies and intensities. In fact, the 5d orbitals of the gold atom lie closer in energy to the 6s orbital than do the 4d orbitals of silver to the 5s. Fig. 6A shows the wavelengths of the longitudinal peak for neutral gold nanowires. A red shift of the longitudinal peak is observed. A similar observation was found at the PW91/LANLDZ level of theory.[35] At the SAOP/DZ level of theory, a break in linearity occurs at ten atoms (eights atoms with LB94/DZ), which is the size where the longitudinal peak becomes distinguishable from the d-based transitions. At that system length, the peak intensity becomes stronger than the intensity of the transitions originating from the d-band. The HOMO–LUMO transition couples with the d-based transitions because they have the same symmetry. As a result, a splitting of the longitudinal peak occurs. We can adjust for this effect by considering the weighted average of the transition dipole moment of the HOMO–LUMO transition from several excitation peaks. As shown in Fig. 7A, the linear relationship between the wavelength of the HOMO–LUMO transition and the number of atoms in the chain is recovered. This shows that the longitudinal transitions of gold nanowires still follow the particle-in-a-cylinder model but the d-band splits the HOMO–LUMO peak. Since the d-band energy does not vary much with size whereas the energy of the longitudinal peak red shifts with length, the energy difference between the d-based transitions and the longitudinal peak increases as the nanowires grows from Au_{10} to Au_{20} and this difference reaches about 1 eV for Au_{20}. However, this energy difference is more than 1 eV smaller than the one discussed previously with the silver nanowires, which can be explained by the stronger coupling between the d-based and HOMO–LUMO transitions. It should be noted that the d-band mixing is also reflected in the intensity of the longitudinal peak. As shown on Fig. 8A, the intensity of the longitudinal peak starts increasing linearly with chain length at 8–10 atoms. This corresponds to the size where the longitudinal peak starts to separate from the d-based transitions.

Contrary to the silver case, a transverse peak can only be distinguished in the two-atom chain. For the longer nanowires, a broad band begins at about 6 eV instead. This band shows a similar pattern for all the nanowires and starts converging at a system length of about twelve atoms. The high-intensity transitions involved are mainly $d\Pi \rightarrow \Pi$ transitions, as shown in Table 2. These transitions arise from localized d-orbitals to delocalized s-based Π orbitals. Because of the symmetry of these transitions, they will be excited by *z*-polarized light. Fig. 5B

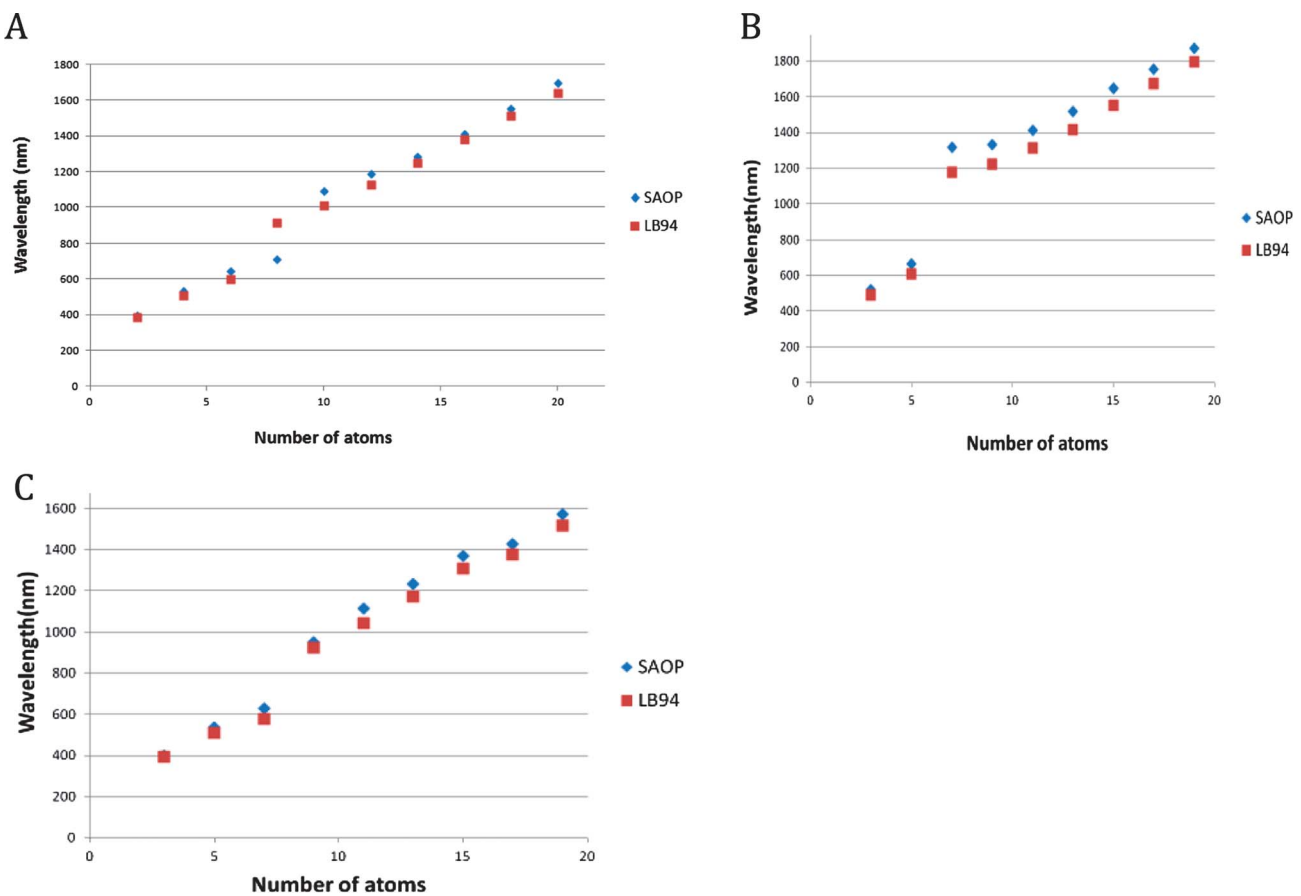

Fig. 6 Wavelengths of main longitudinal peak for (A) neutral (B) positively charged and (C) negatively charged gold nanowires.

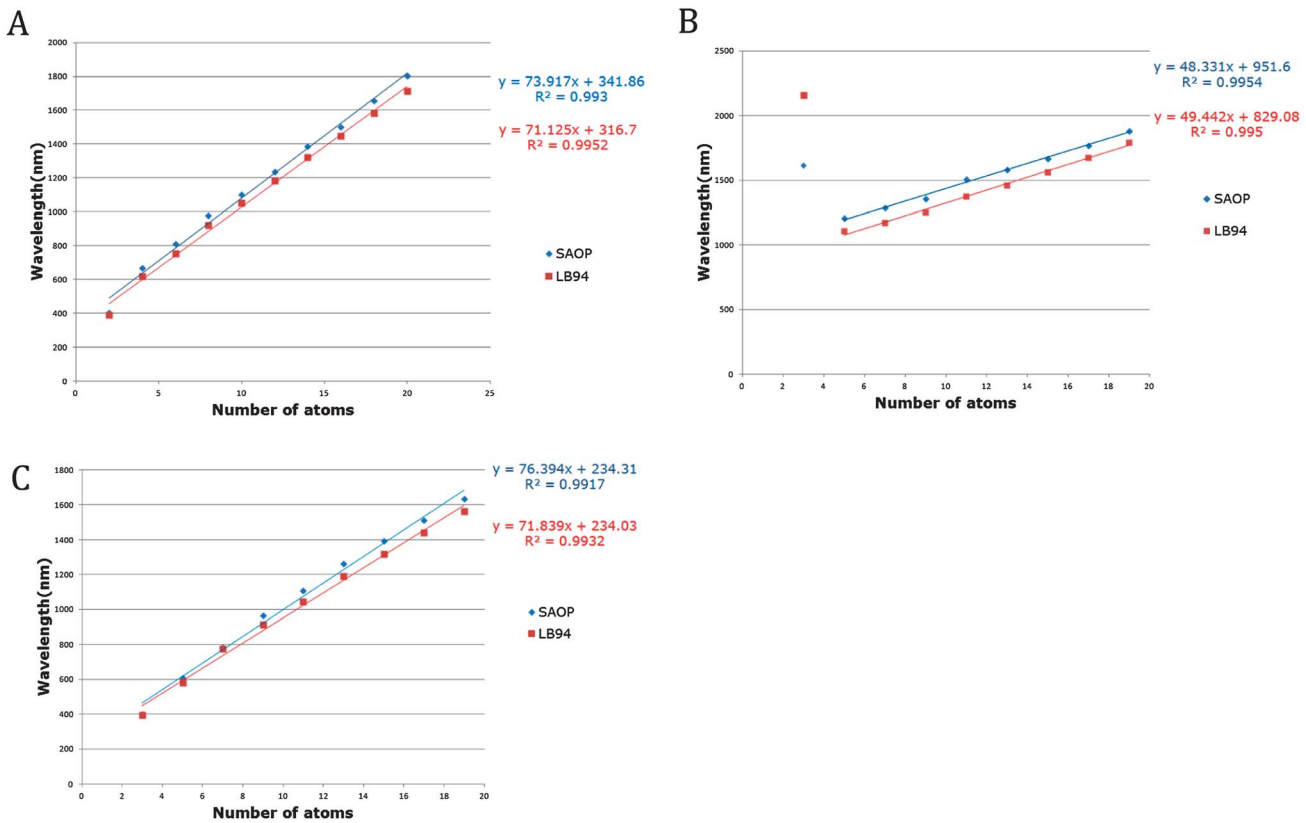

Fig. 7 Weighted average of the HOMO–LUMO transition for (A) neutral (B) positively charged and (C) negatively charged gold nanowires.

displays only the transverse excitations of Au_{20}, which correspond to excitations across the short axis (*xy*-plane). Transverse peaks begin at a wavelength of about 6.3 eV and their oscillator strength is about ten times smaller than the $d\Pi \rightarrow \Pi$ excitation. Those transverse modes are mainly $d\sum \rightarrow \Pi$ and $d\Pi \rightarrow \sum$ transitions and they all have high contributions to the dipole moments, although not quite as high as the $d\Pi \rightarrow \Pi$ transitions (Table 3). The $d\sum \rightarrow \Pi$ and $d\Pi \rightarrow \sum$ transitions are the majority in the 6–7 eV range but they are hidden by a few more intense $d\Pi \rightarrow \Pi$ transitions described above. It should be noted that a band of transverse dipole excitation modes between 5 and 6 eV was previously observed at the PW91/LANL2DZ level of theory with a frozen orbital picture.[35] Moreover, we expect that the intensity of this transverse band would increase as the diameter of the system increases. An investigation of the effect of the diameter on the excitation spectra is currently underway.

Since the d-band is so important for gold species, it is discussed in more detail here. As the wire grows longer, the d-band forms a distinct pattern. In order to study this pattern, all the d-based transitions between the longitudinal peak and transverse band are plotted for the neutral nanowires with 12 to 20 atoms, as shown in Fig. 9. Two main transitions occur at about 2 and 2.8 eV. A series of transitions with lower oscillator strength occur between 3.5 and 5.5 eV. The transition energies shift slightly depending on the size of the nanowires but the overall pattern is apparent. A density of states diagram showing the d orbitals for gold nanowires with 12 to 20 atoms is also shown in Fig. 7. We note that the two figures are practically mirror images of one another. However, the

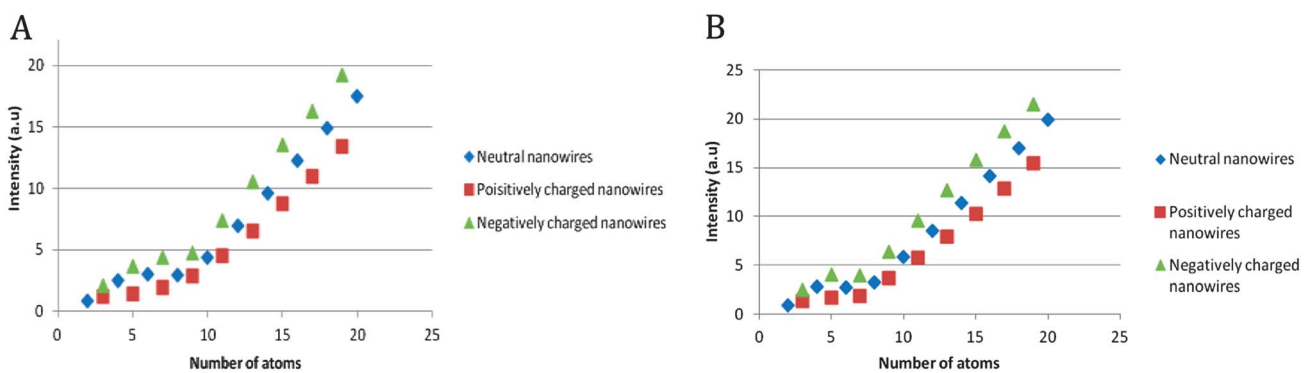

Fig. 8 Oscillator strength of the longitudinal transition energy of gold nanowires with (A) SAOP/DZ and (B) LB94/DZ.

Table 2 Transitions with the highest oscillator strength occurring between 6 and 7 eV for the Au_{20} nanowire

Transition energy (eV)	Oscillator strength	Transition	Weight	Contribution to the dipole moment
5.99	0.76	$80\pi_g \rightarrow 81\pi_u$	0.9530	2.8721
6.10	0.60	$79\pi_g \rightarrow 81\pi_u$	0.5901	−0.1782
		$80\pi_u \rightarrow 81\pi_g$	0.3476	−1.6479
6.28	0.46	$79\pi_u \rightarrow 81\pi_g$	0.5308	0.1957
		$79\pi_g \rightarrow 82\pi_u$	0.3315	1.4809
6.31	0.54	$79\pi_g \rightarrow 82\pi_u$	0.4586	1.7373
6.85	0.52	$78\pi_g \rightarrow 83\pi_u$	0.6392	1.6190

Table 3 $d\sum \rightarrow \Pi$ transitions involved in the transverse band of the Au_{20} nanowire at SAOP/DZ level of theory. The transitions with the highest oscillator strength are considered

Transition energy (eV)	Oscillator strength	Transition	Weight	Contribution to the dipole moment
6.29	0.013	$129\sigma^+_g \rightarrow 81\pi_u$	0.2369	−1.0961
6.43	0.019	$130\sigma^+_g \rightarrow 82\pi_u$	0.5052	−1.4817
6.53	0.030	$130\sigma^+_u \rightarrow 82\pi_g$	0.4212	1.3255
6.62	0.023	$132\sigma^+_g \rightarrow 83\pi_u$	0.4002	1.1708
6.79	0.018	$131\sigma^+_u \rightarrow 83\pi_g$	0.4873	−0.7199

density of states diagram is broader than the excitation spectrum. This can be explained by the fact that the density-of-states diagram includes all the d orbitals (*i.e.* with d_{xy}, d_{xz}, d_{yz}, $d_{x^2-y^2}$ and d_{z^2} character). However, the transitions involved in the excitation spectrum originate from d orbitals with d_{z^2} character. In fact, they are the only d orbitals with the right symmetry to contribute to transitions into LUMO, LUMO + 1, LUMO + 2, LUMO + 3 and LUMO + 4 orbitals, which have $\sum$ character.

(2) Positively and negatively charged nanowires. The positively charged and negatively charged gold nanowires display similar trends as the neutral ones. The wavelength of the longitudinal peak also shows a break in linearity at five atoms for the positively charged systems and at seven atoms for the negatively charged species, as shown in Fig. 6B and C. In a similar manner as the neutral case, linearity is recovered by taking the weighted average of the HOMO–LUMO transition, as shown in Fig. 7B and C. However, Au_3^+ does not fit the trend for the positively charged nanowires. In fact, the HOMO–LUMO transition for this system is at much lower energy. Similarly to the silver case, the wavelength of the HOMO–LUMO transition increases more rapidly with size for the neutral and negatively charged nanowires than for the positively charged nanowires. Also, similarly to the neutral case, the coupling between the HOMO–LUMO transition and the d-band is reflected in the intensity of the longitudinal peak. In fact, there is a bump in the peak intensity between three and seven atoms for the charged species (Fig. 8). After that, the peak intensity varies linearly with the chain length, similarly to the silver case. The d-band pattern is also recovered for the positively charged and negatively charged species. Since these orbitals are fairly localized, this is expected. The transverse band at 6 eV also compares fairly well with the neutral species, which suggests that the transitions involved originate from similar orbitals as the neutral case.

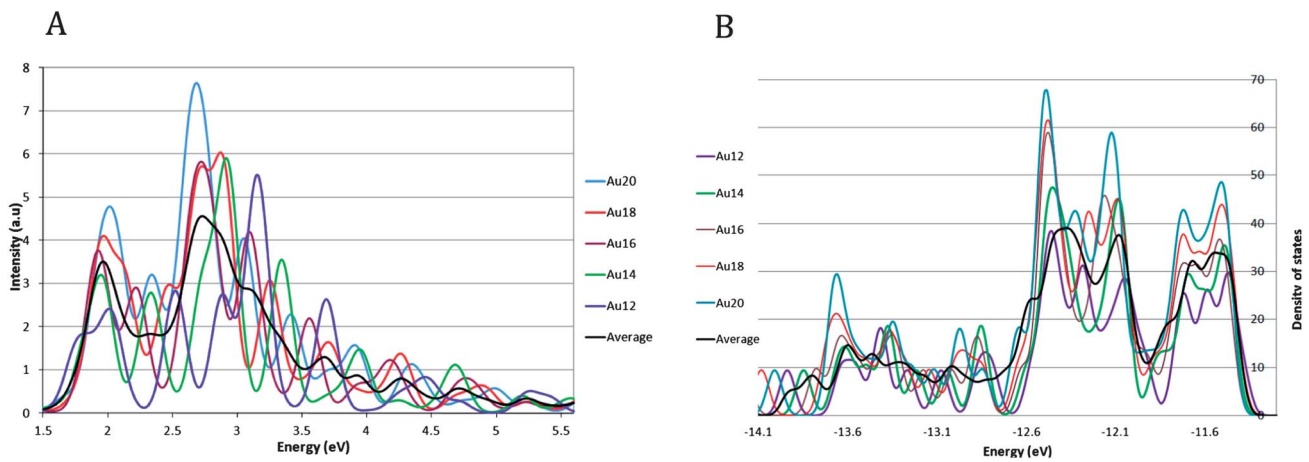

Fig. 9 (A) d-Band of the neutral nanowires starting at a wire length of twelve atoms. (B) Density of states of the d orbitals of gold nanowires. This data was plotted with SAOP/DZ.

Conclusions

The excitation spectra of linear chains of silver and gold have been studied for systems with lengths between two and twenty atoms. Neutral, positively charged, and negatively charged nanowires typically follow the same patterns. For silver, a series of delocalized $\sum_m$ and Π_m orbitals formed from 5s orbitals lie near the HOMO–LUMO gap. Localized 4d-based orbitals are well separated in energy. The excitation spectra for both silver and gold exhibit a main longitudinal peak corresponding to the HOMO–LUMO excitation along the chain. This peak shifts to the red as the chain length increases. The shift is linear for silver, which is consistent with the particle-in-a-cylinder model. However, the d-band of the gold species affects the energy of this peak because of coupling due to symmetry; this can be treated by taking a weighted average of the transition dipole moment contributions for all peaks with some HOMO–LUMO contribution. Silver nanowires show a transverse peak with nearly constant energy that is formed from delocalized $\sum_m \rightarrow \Pi_m$ transitions whose transition dipole moments add in a constructive manner in analogy to the transverse plasmonic peak of larger nanoparticles. Transitions arising from the d-band also tend to contribute to this peak as the chain becomes longer. The gold species show a wide transverse band corresponding to $d\sum \rightarrow \Pi$ and $d\Pi \rightarrow \sum$ transitions. This band is mostly hidden by $d\Pi \rightarrow \Pi$ transitions with oscillator strength about ten times higher than the transverse excitations. Silver nanowires show a low-intensity d-band that essentially goes away for systems of longer length. On the other hand, the excitation spectra of the gold species show a strong d-band that converges to a specific pattern at a chain length of about twelve atoms. This d-band also affects the position of the main longitudinal peak.

Acknowledgements

This material is based upon work supported by the Air Force Office of Scientific Research under AFOSR Award No. FA9550-09-1-0451. C.M.A. also thanks the Alfred P. Sloan Foundation for a Sloan Research Fellowship (2011–2013) and the Camille and Henry Dreyfus Foundation for a Camille Dreyfus Teacher-Scholar Award (2011–2016).

References

1 Z. A. Tagar, Sirajuddin, N. Memon, M. H. Agheem, Y. Junejo, S. S. Hassan, N. H. Kalwar and M. I. Khattak, *Sens. Actuators, B*, 2011, **157**, 430–437.
2 J. Puišo, J. Laurikaitien, D. Adlienė and I. Prosyčeva, *Radiat. Prot. Dosim.*, 2010, **139**, 353–356.
3 Y. Sun, *J. Phys. Chem. C*, 2010, **114**, 2127–2133.
4 T. L. Temple and D. M. Bagnall, *J. Appl. Phys.*, 2011, **109**, 084343.
5 X. Huang, S. Neretina and M. A. El-Sayed, *Adv. Mater.*, 2009, **21**, 4880–4910.
6 X. Huang, I. H. El-Sayed, W. Qian and M. A. El-Sayed, *J. Am. Chem. Soc.*, 2006, **128**, 2115–2120.
7 J. Z. Zhang, *J. Phys. Chem. Lett.*, 2010, **1**, 686–695.
8 H. J. Parab, H. M. Chen, T. Lai, J. H. Huang, P. H. Chen, R. Liu, M. Hsiao, C. Chen, D. Tsai and Y. Hwu, *J. Phys. Chem. C*, 2009, **113**, 7574–7578.
9 S. Link and M. El-Sayed, *J. Phys. Chem. B*, 1999, **103**, 4212–4217.
10 A. L. González, C. Noguez, G. P. Ortiz and G. Rodríguez-Gattorno, *J. Phys. Chem. B*, 2005, **109**, 17512–17517.
11 B. J. Wiley, S. H. Im, Z. Li, J. McLellan, A. Siekkinen and Y. Xia, *J. Phys. Chem. B*, 2006, **110**, 15666–15675.
12 S. Link, M. B. Mohamed and M. A. El-Sayed, *J. Phys. Chem. B*, 1999, **103**, 3073–3077.
13 R. Jin, Y. Cao, C. A. Mirkin, K. L. Kelly, G. C. Schatz and J. G. Zheng, *Science*, 2001, **294**, 1901–1903.
14 S. Fedrigo, W. Harbich and J. Buttet, *Phys. Rev. B: Condens. Matter Mater. Phys.*, 1993, **47**, 10706–10715.
15 A. L. Schmucker, N. Harris, M. J. Banholzer, M. G. Blaber, K. D. Osberg, G. C. Schatz and C. A. Mirkin, *ACS Nano*, 2010, **4**, 5453–5463.
16 J. Tiggesbäumker, L. Köller, K. Meiwes-Broer and A. Liebsch, *Phys. Rev. A: At., Mol., Opt. Phys.*, 1993, **48**, R1749–R1752.
17 P. K. Jain and M. A. El-Sayed, *Chem. Phys. Lett.*, 2010, **487**, 153–164.
18 S. A. Khan, D. Senapati, T. Senapati, P. Bonifassi, Z. Fan, A. K. Singh, A. Neeley, G. Hill and P. C. Ray, *Chem. Phys. Lett.*, 2011, **512**, 92–95.
19 L. Koponen, L. O. Tunturivuori, M. J. Puska and Y. Hancock, *J. Chem. Phys.*, 2010, **132**, 214301.
20 C. M. Aikens, *J. Phys. Chem. Lett.*, 2011, **2**, 99–104.
21 C. M. Aikens, S. Li and G. C. Schatz, *J. Phys. Chem. C*, 2008, **112**, 11272–11279.
22 M. Liao, P. Bonifassi, J. Leszczynski, P. C. Ray, M. Huang and J. D. Watts, *J. Phys. Chem. A*, 2010, **114**, 12701–12708.
23 M. Harb, F. Rabilloud, D. Simon, A. Rydlo, S. Lecoultre, F. Conus, V. Rodrigues and C. Felix, *J. Chem. Phys.*, 2008, **129**, 194108.
24 X. Hou, X. Zhang, S. Chen, Y. Fang, N. Li, X. Zhai and Y. Liu, *Colloids Surf., A*, 2011, **384**, 345–351.
25 M. Szymańska-Chargot, A. Gruszecka, A. Smolira, K. Bederski, K. Gluch, J. Cytawa and L. Michalak, *J. Alloys Compd.*, 2009, **486**, 66–69.
26 A. Sánchez-Iglesias, I. Pastoriza-Santos, J. Pérez-Juste, B. Rodríguez-González, F. J. García de Abajo and L. M. Liz-Marzán, *Adv. Mater.*, 2006, **18**, 2529–2534.
27 D. Seo, C. I. Yoo, I. S. Chung, S. M. Park, S. Ryu and H. Song, *J. Phys. Chem. C*, 2008, **112**, 2469–2475.
28 M. Kasture, M. Sastry and B. L. V. Prasad, *Chem. Phys. Lett.*, 2010, **484**, 271–275.
29 A. M. A. El-Sayed, *Mater. Chem. Phys.*, 2010, **121**, 349–353.
30 W. Ni, T. Ambjörnsson, S. P. Apell, H. Chen and J. Wang, *Nano Lett.*, 2009, **10**, 77–84.
31 J. Yan and S. Gao, *Phys. Rev. B: Condens. Matter Mater. Phys.*, 2008, **78**, 235413.
32 J. Yan, Z. Yuan and S. Gao, *Phys. Rev. Lett.*, 2007, **98**, 216602.
33 H. Kim, C. Xiang, A. G. Güell, R. M. Penner and E. O. Potma, *J. Phys. Chem. C*, 2008, **112**, 12721–12727.
34 V. V. Kresin, *Phys. Rev. B: Condens. Matter Mater. Phys.*, 1995, **51**, 1844–1849.
35 K. Lian, P. Salek, M. Jin and D. Ding, *J. Chem. Phys.*, 2009, **130**, 174701.
36 G. te Velde, F. M. Bickelhaupt, E. J. Baerends, C. Fonseca Guerra, S. J. A. van Gisbergen, J. G. Snijders and T. Ziegler, *J. Comput. Chem.*, 2001, **22**, 931–967.
37 A. D. Becke, *Phys. Rev. A: At., Mol., Opt. Phys.*, 1988, **38**, 3098.
38 J. P. Perdew, *Phys. Rev. B: Condens. Matter Mater. Phys.*, 1986, **33**, 8822.
39 E. van Lenthe, E. J. Baerends and J. G. Snijders, *J. Chem. Phys.*, 1994, **101**, 9783–9792.
40 E. van Lenthe, A. Ehlers and E. Baerends, *J. Chem. Phys.*, 1999, **110**, 8943–8953.
41 P. R. T. Schipper, O. V. Gritsenko, S. J. A. van Gisbergen and E. J. Baerends, *J. Chem. Phys.*, 2000, **112**, 1344–1352.
42 R. van Leeuwen and E. J. Baerends, *Phys. Rev. A: At., Mol., Opt. Phys.*, 1994, **49**, 2421–2431.
43 H. E. Johnson and C. M. Aikens, *J. Phys. Chem. A*, 2009, **113**, 4445–4450.
44 J. Duan, K. Park, R. I. MacCuspie, R. A. Vaia and R. Pachter, *J. Phys. Chem. C*, 2009, **113**, 15524–15532.
45 L. Hu, H. S. Kim, J. Lee, P. Peumans and Y. Cui, *ACS Nano*, 2010, **4**, 2955–2963.
46 C. Gao, Q. Zhang, Z. Lu and Y. Yin, *J. Am. Chem. Soc.*, 2011, **133**, 19706–19709.

